Journal of The Electrochemical Society, **153** (10) A1971-A1978 (2006)
0013-4651/2006/153(10)/A1971/8/$20.00 © The Electrochemical Society

Liquid Water Storage, Distribution, and Removal from Diffusion Media in PEFCS

J. J. Kowal, A. Turhan,* K. Heller, J. Brenizer, and M. M. Mench,z**

Fuel Cell Dynamics and Diagnostics Laboratory, Radiation Science and Engineering Center and Department of Mechanical and Nuclear Engineering, The Pennsylvania State University, University Park, Pennsylvania 16802, USA

Liquid water storage in the diffusion media (DM) of polymer electrolyte fuel cells (PEFCs) is a function of design geometry, surface geometry, and operating conditions, and the DM, water storage, and can affect transient response, degradation via ionic contaminants, pressure loss, and freeze–thaw behavior. Neutron imaging was used to quantify the liquid water distribution in a PEFC under a variety of flow rates, humidities, and currents with paper or cloth DM. For a wide range of conditions, the paper DM held roughly 60% of the total water stored under the landings and the remaining 40% in, or under, the channels. The cloth DM had a nearly 50:50 channel to land liquid water distribution. From 0.2 to 1.0 A/cm^2 current conditions, the paper DM held 174% more water per volume of DM under the landings than cloth, resulting in a very high liquid saturation and eventual flooding. Increasing flow rate decreased the total liquid water content, mostly from removal of droplets. The residual liquid water under the lands was removed with increased flow rate more readily using the cloth DM, thus it was a more effective material for low power purge. Transient testing showed the time scale of significant liquid water accumulation is on the order of minutes.
 [DOI: 10.1149/1.2258049]

Manuscript submitted January 13, 2006; revised manuscript received June 5, 2006. Available electronically August 28, 2006.

The management of water within a polymer electrolyte fuel cell (PEFC) is particularly challenging. Loss of only a fraction of a milligram of water per cm^2 superficial active area within a catalyst layer can cause performance loss via electrode dry-out.[1] The presence of excess liquid water flooding the catalyst layer can increase resistance of reactant transport to the electrode surface, also causing severe performance loss. Even if the catalyst layer is relatively liquid-free, liquid water in the diffusion media (DM) or flow channels can also limit performance via blockage of reactant. A recent study suggests that for a hydrophobic catalyst layer and diffusion media, the diffusion media flooding precedes any catalyst layer flooding.[2] Thus, diffusion media flooding needs to be more thoroughly studied before an optimized structure can be proposed or complex models are complete.

The DM serves many purposes in a hydrogen-air PEFC, including (*i*) transport of reactants from the flow channels to the electrodes, (*ii*) removal of vapor- and liquid-phase water produced in the cell, (*iii*) transport of electrons to and from the electrodes, (*iv*) structural support of the membrane electrode assembly (MEA), and (*v*) transport of waste heat.[3,4] Adequate water in the membrane electrolyte and catalyst layers is important for suitable performance, but the steady-state liquid water content stored in the DM during operation is also of interest, in terms of freeze/thaw, start-up, degradation, and purging, because the DM can typically store much more water than any other component besides the flow channels.

Residual water storage during operation is also of critical importance for system transients. Although steady-state performance, especially at low current densities, can be nearly identical for different DM, a higher residual water storage in a given DM retards thermal transients, can result in additional damage during freeze/thaw, and can act as a conduit for ionic impurities which degrade the electrode and electrolyte. This residual water mass at minimum requires additional energy to remove via purge. Thus, it is desirable to find the DM with the lowest residual water content in steady state and the least energy-intensive purge procedure. The prediction of PEFC performance and water distribution has been modeled many times in literature. [5-21] Although these models have been used to successfully predict flooded performance in PEFCs, they are quite complex, validation data are scarce, and few currently have the capacity to delineate between varieties of DM, other than by fitting a bulk contact angle representing the average surface energy of the media, or the empirically derived terms in a saturation/capillary pressure Leverette function relationship.

Experimentally, several ex situ and in situ experimental studies have been employed to measure the water content in a fuel cell or visualize its motion.[22-25] However, most of these studies have utilized special cells that may change cell operating characteristics. For example, optical cells must be built with transparent materials not typically used in PEFCs, and the thermal or current collection boundary conditions are difficult to control. Ex situ methods are valuable for analyzing a single component, but fuel cells are very dependent on a particular system and the compression, materials, and interfacial properties between media so that complementary in situ methods are still needed. A fairly powerful in situ technique for studying the liquid water distribution of PEFCs is neutron imaging.[26-30] Neutron imaging can provide high-resolution visualization of fuel cells made from common fuel cell materials. Recently, quantified water distribution with high-precision real-time video has been demonstrated.[31]

Experimental

This study was conducted at the Breazeale Nuclear Reactor at the Penn State Radiation Science and Engineering Center. All tests were performed at a reactor power of 1000 kW. At this power level, the thermal neutron flux at the imaging plane is 1.4×10^7 n cm^{-2} s^{-1} with a linear defect (LD) of $\sim$150, providing a neutron beam of sufficient intensity for radioscopic purposes. All images were captured by an imaging system comprised of a Thompson tube and 1004×1004 pixel charge-coupled device (CCD) camera with a 10-bit depth and then recorded on a specialized computer, capable of achieving capture rates of up to 30 frames per second. This system provides spatial resolutions down to 129 μm and detection of liquid water layers greater than 13 μm thick. Further specifications of the reactor, the thermal neutron beam it provides, and the imaging system can be found in Turhan et al.[1,29,31]

The fuel cell used in these tests has a seven-channel parallel flow field and an active area of 12.5 cm^2, as shown in Fig. 1a and b. The oxidizer and fuel streams were counter flow, and all the experiments were conducted at a back pressure of 100 kPa gauge. The cell temperature was controlled by a thermocouple in the cathode control plate located approximately 5 mm from the cathode flow field, two 10 mm cartridge heaters inserted in the fuel cell backing plates, and an Omega proportional integral differential (PID) digital controller. An external forced convection system was used to actively cool the external surface and maintain constant temperature. The flow rate,

* Electrochemical Society Student Member.
** Electrochemical Society Active Member.
z E-mail: mmench@psu.edu

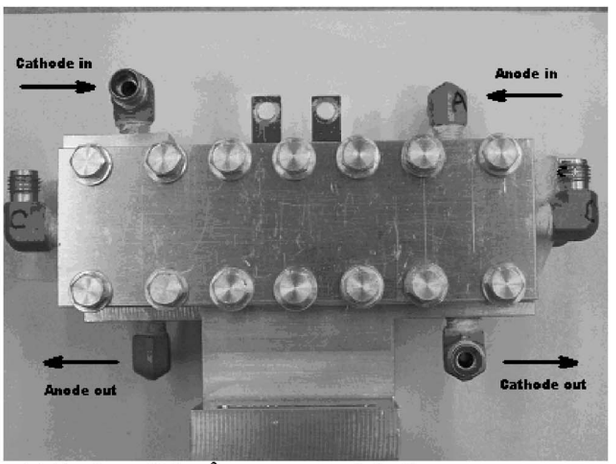

(a) Aluminum, 12.5 cm^2, countercurrent fuel cell.

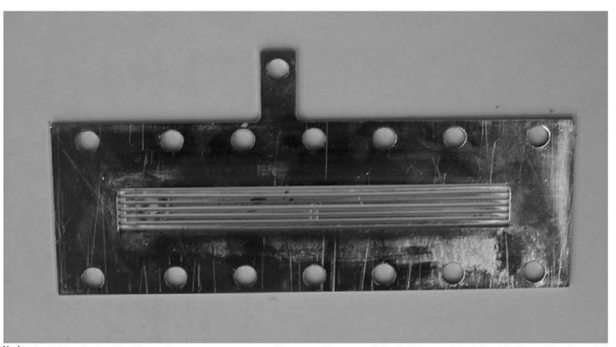

(b) Gold-plated aluminum, seven channel, parallel flow field of the fuel cell.

Figure 1. Photos of (a) fuel cell and (b) current collecting plate of the fuel cell used in this study.

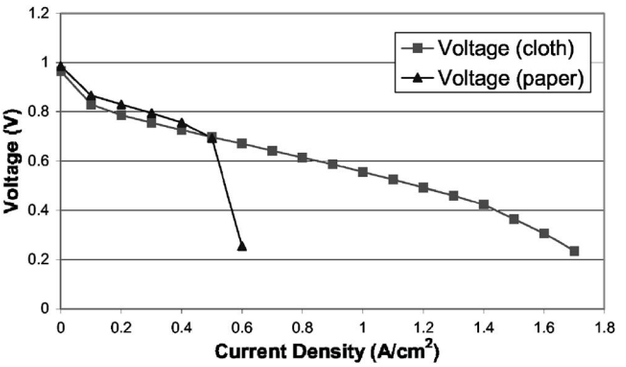

Figure 2. Polarization curves for paper and cloth DM. Test conditions: T_{cell} = 80°C, P_{cell} = 0.1 MPag, Flow rate A/C = 436/1040 sccm, RH A/C = 90/80°C.

inlet relative humidity control, and pressure control were all used as specified in Turhan et al.[1] The current and voltage of the cell was controlled using a Lynntech, Inc. loadbank.

Both steady-state and transient tests were performed in these experiments, as are shown in Tables I and II. Each steady-state test (Table I) consisted of taking sixty frames of video data at five frames per second and averaging them to reduce the random noise seen in a single frame. The fuel cell was operated for 30 min before each test at the given test conditions to achieve steady state. For the paper DM, severe flooding losses occurred in steady state for current densities above 0.5 A/cm^2 100% relative humidity (RH). Figure 2 shows the steady-state (>30 min time at each data point) polarization curves for the cloth and paper DM at 100% RH, 7.5 psig cell pressure, and flow rates of 436 sccm for the anode and 1040 sccm

Table I. Operating conditions for steady-state tests (each completed for cloth and paper DM, 20 tests total).

Test no.	Current density (A/cm^2)	Cell temp (°C)	Line temp (°C)	Anode flow rate (sccm)	Cathode flow rate (sccm)	Anode hum. temp (°C)	Cathode hum. temp (°C)
1	0.2	80	100	174	417	90	80
2	0.2	80	100	174	417	Dry	80
3	0.35	80	100	174	417	90	80
4	0.35	80	100	436	1040	90	80
5	0.7[a]	80	100	174	417	90	80
6	0.7	80	100	174	417	Dry	80
7	0.7[a]	80	100	436	1040	90	80
8	0.7	80	100	436	1040	Dry	80
9	1[a]	80	100	174	417	90	80
10	1[a]	80	100	436	1040	90	80

[a] For paper DM, flooding losses occurred over 30 min time of measurement so that at steady state, current density shown was not achievable.

Table II. Operating conditions for transient tests performed on cloth diffusion media.

Test no.	Current density (A/cm^2)	Duration (s/step)	Cell temp (°C)	Line temp (°C)	Anode flow rate (sccm)	Cathode flow rate (sccm)	Anode hum. temp (°C)	Cathode hum. temp (°C)
11	0.2–0.7	1	60	100	174	417	90	80
12	0.2–0.7	1	80	100	174	417	90	80
13	0.2–0.7	10	60	100	174	417	90	80
14	0.2–0.7	10	80	100	174	417	90	80
15	0.2–0.7	20	60	100	174	417	90	80
16	0.2–0.7	20	80	100	174	417	90	80
17	0.2–1.0	1	60	100	436	1040	90	80
18	0.2–1.0	1	60	100	436	1040	90	Dry
19	0.2–1.0	1	80	100	436	1040	90	80
20	0.2–1.0	1	80	100	436	1040	90	Dry

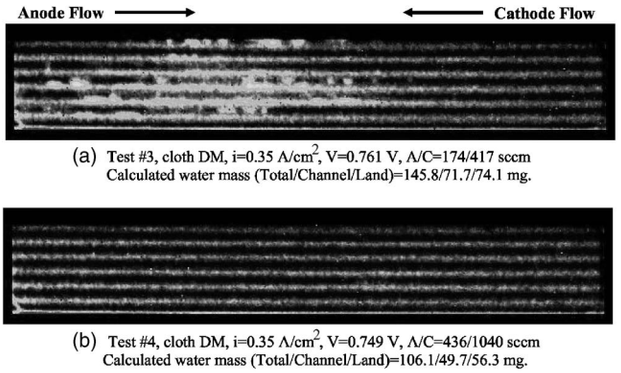

Figure 3. Neutron radiography images at (a) low flow rate and (b) high flow rate. Test conditions: T_{cell} = 80°C, P_{cell} = 0.1 MPag, RH A/C = 90/80°C.

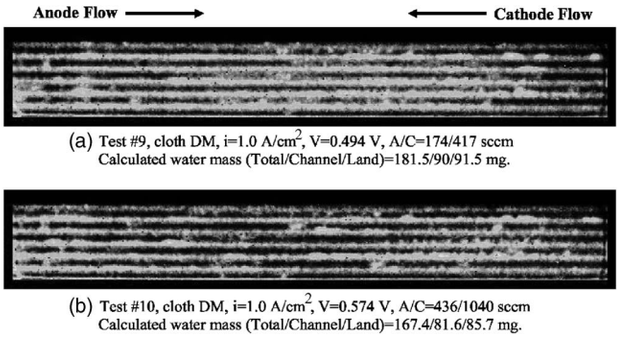

Figure 5. Neutron radiography images at (a) low flow rate and (b) high flow rate. Test conditions: T_{cell} = 80°C, P_{cell} = 0.1 MPag, RH A/C = 90/80°C.

for the cathode. The cloth DM was able to operate under much higher current densities in these tests. For the flooded paper DM conditions noted in Table I, data were still taken for the paper tests after 30 min. However, due to the gradual accumulation of water, the performance of the cell fell to low levels. The data on liquid-water accumulation taken are expected to be accurate, however, because the water content in the DM that resulted in the flooding should not change much after flooding loss shutdown.

The transient cloth DM tests (Table II) were analyzed by taking a continuous stream of images at five frames per second throughout the test. The data were then analyzed using a three-frame moving average (i.e., averaging a frame with the frame before it and the frame after it). This yields adequate temporal resolution while still reducing the random noise. The current density was varied from 0.2 to 0.7 A/cm^2 by 0.1 A/cm^2 increments for all the transient tests. The current was held constant at each step for 1, 10, or 20 s for each. A 5 s gap was left between each step test for the 10 and 20 s step tests in order to step up the current of the fuel cell via the computer load bank control system.

An analysis software program developed by Pennsylvania State University (PSU), called *PSUMagic*, processed the data from all tests.[31] Through the acquisition and use of a dry image, an image of the cell in operation, and an image of the neutron beam itself, *PSUMagic* was used to digitally apply noise reduction, beam intensity compensation between images, beam shape correction, and background removal to ultimately quantify the water mass observed in the operating fuel cell image. *PSUMagic* was used to quantify the observed water on a pixel-by-pixel basis through the use of a grayscale vs water thickness look-up table. This look-up table was generated from the grayscale values of a variable-thickness water calibration wedge imaged with the cell via a technique published by Brenizer et al.[32]

Error values associated with quantified water masses are calculated based on pixel grayscale fluctuations. By observing the raw data from a test, *PSUMagic* is capable of associating a statistical error with each pixel in an image. The statistical error is tracked throughout the processing procedure and applied during water quantification. The statistical fluctuation, when applied to water quantification tests involving an aluminum block with milled, water-filled channels of known dimensions, suggests water mass errors of less than approximately 6.5%.[31] The same level of error is therefore taken to be applicable to the fuel cell data.

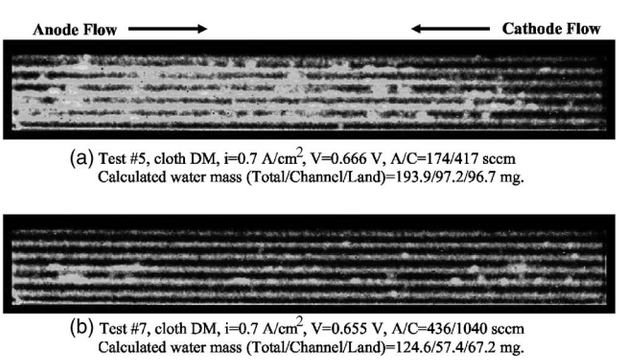

Figure 4. Neutron radiography images at (a) low flow rate and (b) high flow rate. Test conditions: T_{cell} = 80°C, P_{cell} = 0.1 MPag, RH A/C = 90/80°C.

Results and Discussion

Flow rate effect.— Figures 3-5 show the neutron images of tests 3 and 4, 5 and 7, and 9 and 10, respectively, from Table I for the cloth DM. These three pairs of tests were performed at different currents using overhumidified inlet conditions to compare the low flow rate with the higher flow rate condition for two DM materials. One was a hydrophobic carbon woven fiber cloth with a thickness of 250 μm, and the other was a hydrophobic carbon nonwoven fiber paper with a thickness of 180 μm. The three pairs of tests compare a low flow rate (A/C = 174/417 sccm, stoichiometry of 2 for both electrodes at 1 A/cm^2) with a flow rate 2.5 times higher (A/C = 436/1040 sccm, stoichiometry of 5 for both electrodes at 1 A/cm^2) for 0.35, 0.7, and 1.0 A/cm^2 and overhumidified inlet initial conditions. Water tends to collect under the landings of the fuel cell in either high or low flow rates,[1,29] leaving what looks like a rough image of the flow field in the colorized images.[a] At the lower flow rate, there is a significant amount of channel water, indicated by the slugs seen in the channels in Fig. 3a, 4a, and 5a. At the higher flow rate, the slugs are more easily removed by drag forces and the slug density in the channels is reduced. It cannot be determined from the neutron images alone whether the water seen in the channel is actually in the channel or in the DM underneath the channel because it is a 2D line integral image from anode to cathode. However, in the case of many of the other visible slugs, the equivalent water thickness is greater than the maximum water thickness of both DMs, so that a portion of this liquid must be in the channel. In every case the total, channel, and land water content was less at the high flow rate condition, as seen in Table III. This indicates that there is at least some water in the channel itself and not in the DM under the channel. If the water were entirely in the DM, a higher flow rate fully humidified condition would not be able remove the liquid water as effectively. The evidence also suggests that some of the water in the channel is in droplet form and does not solely exisit as a continuous film around the hydrophilic channel, as sketched in Fig. 6. If most of

[a] See www.mne.psu.edu/fuelcell/neutron.pdf for color images of all tests 1–10 for paper and cloth in steady state.

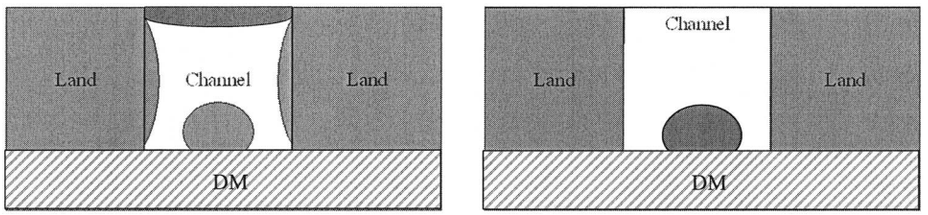

Figure 6. Schematics of possible water geometries.

the channel level water were in film form along the walls of the channel, it would be more difficult to remove convectively than slug droplet flow.

Table IV shows the decrease of water from the low-flow-rate case to the high-flow-rate case for the three pairs of tests, in the three regions of interest (total, channel, and lands) and for the two different types of DM. The percent liquid water decrease is defined in Eq. 1 as

$$\% \text{ decrease} = \frac{m_{l,\mathrm{H_2O}}(\text{low flow rate}) - m_{l,\mathrm{H_2O}}(\text{high flow rate})}{m_{l,\mathrm{H_2O}}(\text{low flow rate})} \times 100\% \quad [1]$$

The water decrease percentage was greater in the channel than under the land for all the cases because of the slug removal from the channel via the flow-rate increase. The steady-state residual liquid water under the lands also decreased for every case, indicating water under the lands is flowing from the DM out into the channel at the higher flow condition. Because the flow in these cases is overhumidified at the anode, and fully humidified at the cathode inlet, this is likely due to droplet emergence and subsequent removal from the DM by capillary flow, not evaporative losses. It is particularly interesting that the water decrease under the lands is greater for the cloth DM than the paper DM for all current densities. This is particularly useful information for purging and freeze/thaw considerations because a minimum of residual water is desired in the cell before shutdown to hasten start up and prevent degradation. In these cases, the cloth DM was uniformly more effective than the paper DM at removing more stored water during a flow-rate increase. While we can speculate about the reason for this significant difference, based on in-plane relative permeability or other effect, more fundamental research is needed to understand two-phase flow through different DM.

Diffusion media material effect.— Because the same ten tests were performed for both DM materials, the conditions of which are given in Table I, comparisons can be made between the paper and cloth DM. Note again that for the fully humidified paper tests, flood-

Table III. Liquid-water mass distribution for paper and cloth DM steady-state tests.

		Paper			Cloth		
Test no.	i (A/cm^2)	Total water mass (mg)	Channel water mass (mg)	Land water mass (mg)	Total water mass (mg)	Channel water mass (mg)	Land water mass (mg)
1	0.20	203	85	118	197	97	100
2	0.20	168	67	101	163	80	83
3	0.35	144	51	93	146	72	74
4	0.35	136	46	90	106	50	56
5	0.70	207[a]	89[a]	120[a]	194	97	97
6	0.70	191	77	114	223	116	107
7	0.70	144[a]	49[a]	95[a]	125	57	67
8	0.70	145	50	95	130	61	69
9	1.00	185[a]	74[a]	111[a]	182	90	92
10	1.00	169[a]	63[a]	106[a]	167	82	86
	Averages	169	65	104	163	80	83

[a] For paper DM, flooding losses occurred over 30 min time of measurement so that at steady state, current density shown was not achievable.

Table IV. Residual water decrease from low to high flow rate for paper and cloth DM.

			Paper			Cloth		
Test no.	Cathode flow rate (sccm)	Current density (A/cm^2)	Total water decrease (%)	Channel water decrease (%)	Land water decrease (%)	Total water decrease (%)	Channel water decrease (%)	Land water decrease (%)
3	417	0.35	5.3	10.0	2.8	27.2	30.7	24.0
4	1040	0.35						
5	417	0.7	30.6[a]	45.3[a]	20.7[a]	35.7	40.9	30.5
7	1040	0.7						
9	417	1.0	8.9[a]	14.9[a]	4.9[a]	7.8	9.3	6.3
10	1040	1.0						

[a] For paper DM, flooding losses occurred over 30 min time of measurement so that at steady state, current density shown was not achievable.

Table V. Comparison of diffusion media for three regions. The values for each cloth region (total, channel, and landing) are divided by the corresponding paper region value.

Test no.	Cloth vs paper total (%)	Cloth vs paper channels (%)	Cloth vs paper lands (%)
1	97	114	85
2	97	119	82
3	101	140	80
4	78	108	62
5	94[a]	109[a]	81[a]
6	117	151	94
7	87[a]	118[a]	71[a]
8	90	121	73
9	98[a]	122[a]	83[a]
10	99[a]	130[a]	81[a]
Average	96	123	79

[a] For paper DM, flooding losses occurred over 30 min time of measurement so that at steady state, current density shown was not achievable.

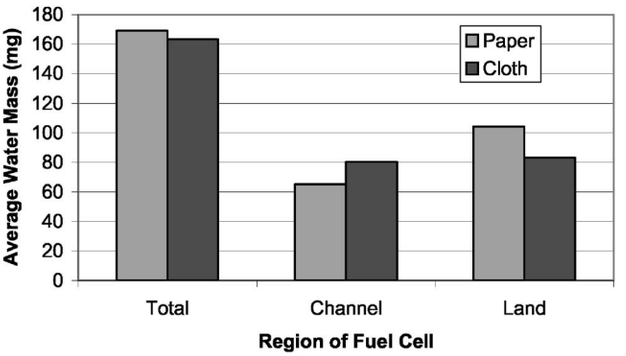

Figure 7. Average water mass values for the three regions of the fuel cell for all ten tests.

ing occurred after several minutes in steady state at a current density greater than 0.5 A/cm^2. All tests were conducted at constant current, except when it was not achievable due to flooding (i.e., cases 5, 7, 9, and 10 for the paper DM in Table I). In these cases the cell was held at the limiting current density as long as possible before dropping to zero. Because the flooded water content was not purged or changed before the images were taken at 30 min, and the current was nearly zero after a flooded state was reached, the water content measured is expected to be an accurate representation of the residual water obtained in this operating condition. Several differences arose from comparison of the data. In Table V, the total cloth residual steady-state water mass values were divided by the similar values for paper in the overall, channel, and landing regions. Interestingly, for all the tests, the total amounts of residual water stored in the fuel cell at a given condition are approximately the same for the cloth and the paper DM, with an average of about 96%, meaning the cloth has slightly less stored water in steady state than the paper DM over the wide range of flow rate, humidity, and current density conditions tested. For the channel region, however, the cloth has approximately 123% of the water compared to the paper under all the test conditions. For the landing region, the cloth has about 79% of the water compared to the paper. This means that, although the overall water content stored in the fuel cell under steady state tends to be the same for both DM materials, more of the liquid water in the cloth DM tends to be in the channel, or in the DM under the channel, than the paper DM. This point is also illustrated in Fig. 7, a comparison of the average water masses for the ten tests. For the cloth DM, the water is roughly split evenly between the channel area and the landing area. For the paper DM, about 40 mg (about 25% of the total liquid water in the cell) more water is under the landings compared to the channel region. Again note the total water is roughly equal for both DM but the distribution is quite different, depending on the DM, given the same gold-plated hydrophilic channel conditions in the fuel cell.

These absolute results are a comparison of the total liquid-water content, not accounting for the different compressed thicknesses and resulting decreased pore volume of the DMs. Assuming a 20% compression over the entire DM, and using the appropriate area (total, channel, and landing), the water mass values can be normalized to examine and compare the relative water storage properties of each DM on an available pore volume basis. The absolute water mass values in Table III were converted to compressed volume normalized liquid-water mass values as shown in Table VI by dividing the total liquid-water mass by the active area of interest (total, channel, and landing) and multiplying by the compressed DM thickness. The average total liquid water storage per cm^3 of compressed DM is 653 mg/cm^3 for cloth and 940 mg/cm^3 for paper for all test conditions. This is not a totally appropriate comparison because it assumes all of the liquid recorded is in the DM, with no water in the channel. Instead, the most appropriate metric is comparison of liquid water observed only under the lands, because it must be in the DM,

Table VI. Compressed-pore volume-normalized water densities for paper and cloth DM steady-state tests.

	Paper, normalized			Cloth, normalized		
Test no.	Total water mass (mg/cm^3)	Channel water mass (mg/cm^3)	Land water mass (mg/cm^3)	Total water mass (mg/cm^3)	Channel water mass (mg/cm^3)	Land water mass (mg/cm^3)
1	1127	876	1420	789	719	870
2	933	695	1210	652	595	718
3	799	527	1118	583	533	642
4	757	475	1087	424	369	488
5	1149[a]	919[a]	1440[a]	776	722	838
6	1063	795	1377	893	863	928
7	797[a]	502[a]	1142[a]	498	426	582
8	807	520	1141	520	452	596
9	1027[a]	763[a]	1335[a]	726	669	793
10	936[a]	650[a]	1270[a]	670	606	743
Averages	940	672	1254	653	595	720

[a] For paper DM, flooding losses occurred over 30 min time of measurement so that at steady state, current density shown was not achievable.

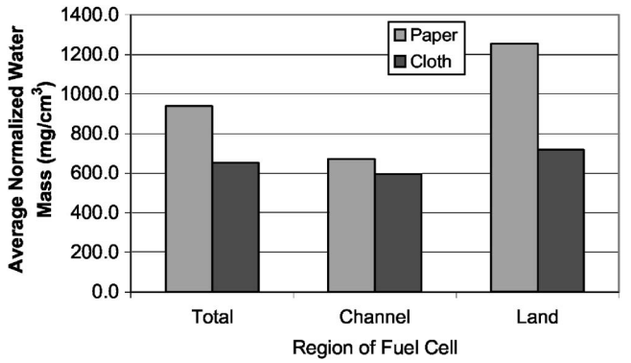

Figure 8. Average normalized water mass values per unit volume of compressed DM for all ten tests.

electrolyte, or catalyst layers, with an overwhelming majority of the storage in the DM. Under the lands, the hydrophobic paper DM averages 1.25 g/cm^3 liquid water and 0.72 g/cm^3 for the cloth DM. Each test condition obviously has different steady-state saturation values, but the paper DM consistently averages 177% the water content under the lands compared to the cloth DM over the wide range of conditions tested. This also renders the paper DM more difficult to purge to the same steady-state condition compared to cloth. Volume-normalized water mass values for the three different regions are shown in Fig. 8. The cloth tends to store less water on a volume basis, and hence maintains a lower saturation level than the paper. However, the paper and cloth DM maintain more liquid water under the lands than in or under the channels for this range of test conditions.

Table VII shows the distribution of liquid water in the cell by dividing the channel and land water masses by the total water mass. The paper DM has about 20% more water under the lands than in or under the channels over the range of conditions tested. In every case, the percentages are very close to the averages of the ten tests for the highly varied conditions. The same calculations for the cloth DM show an average land water percentage of 51% and channel water percentage of 49%. The results of all ten tests are very close to the average, which cover a wide variety of current, humidity, and flow-rate conditions, so the distribution of the water between the channels and the lands is approximately constant for a given DM, in a global sense.

Table VII. Location of water for different diffusion media. The channel or land value (as indicated) for each DM is divided by the total liquid-water value recorded.

Test no.	% Water channels, paper	% Water lands, paper	% Water channels, cloth	% Water lands, cloth
1	41.8	58.2	49.1	50.9
2	40.1	59.9	49.2	50.8
3	35.5	64.6	49.2	50.8
4	33.7	66.3	46.8	53.1
5	43.1[a]	57.8[a]	50.1	49.9
6	40.3	59.8	52.0	48.0
7	33.9[a]	66.1[a]	46.1	53.9
8	34.7	65.3	46.8	52.9
9	40.0[a]	60.0[a]	49.6	50.4
10	37.4[a]	62.6[a]	48.7	51.2
Average	38.1	62.0	48.8	51.2

[a] For paper DM, flooding losses occurred over 30 min time of measurement so that at steady state, current density shown was not achievable.

Table VIII. Calculated cathode DM effective porosity values for compressed DM. A negative value reflects that some liquid-water content must be in the anode DM as well.

	Paper, t = 180 μm (uncompressed)		Cloth, t = 250 μm (uncompressed)	
Test no.	Land water mass (mg)	Effective porosity, lands	Land water mass (mg)	Effective porosity, lands
1	118	−0.51	100.4	−0.07
2	100.5	−0.34	82.8	0.05
3	92.9	−0.27	74.1	0.11
4	90.3	−0.24	56.3	0.24
5	119.6[a]	−0.52[a]	96.7	−0.04
6	114.4	−0.47	107.1	−0.12
7	94.9[a]	−0.29[a]	67.2	0.16
8	94.8	−0.29	68.8	0.15
9	110.9[a]	−0.44[a]	91.5	−0.01
10	105.5[a]	−0.39[a]	85.7	0.03
Averages	104.2	−0.38	83.1	0.05

[a] For paper DM, flooding losses occurred over 30 min time of measurement so that at steady state, current density shown was not achievable.

Using the area under the lands (A_{lands}), the amount of liquid water measured under the lands ($m_{H_2O,\text{lands}}$), the compressed porosity ($\varepsilon_{\text{comp}}$), and the density of water (ρ_{H_2O}), and the thickness of the DM (t), the effective porosity under the landings ($\varepsilon_{\text{eff,lands}}$) can be found using Eq. 2

$$\varepsilon_{\text{eff,lands}} = \frac{V_{o,\text{pores}} - V_{H_2O}}{V_{\text{tot}}} = \left(1 - \frac{m_{H_2O,\text{lands}}}{\varepsilon_{\text{comp}}\rho_{H_2O}A_{\text{lands}}t}\right) \times \varepsilon_{\text{comp}} \quad [2]$$

where A_{lands} is calculated by multiplying the total area by the fraction of the area that is under the landings.

The landing area is used because all the water observed under the landings is in the DM, electrolyte, or catalyst layers on the anode or cathode, but planar neutron imaging cannot be used to distinguish between DM and channel for the channel areas. Also, the DM may protrude into the channel depending on the level of compression and assembly. Therefore, the landing area is the most appropriate region to use for this calculation. The volume of liquid water recorded is subtracted from the compressed volume of pores to calculate the effective porosity under the landings. Table VIII shows the results of this calculation done for all 20 conditions for paper and cloth DM. The water mass is assumed to completely reside in the cathode DM as a worst-case scenario, so the tests with negative values of effective porosity indicate liquid exists in both the anode and cathode DM, because the total water in the catalyst layers and electrolyte is comparatively very small. This is the case for all of the paper tests and four of the cloth tests for two reasons. First, as mentioned above, the liquid water in the paper DM has a tendency to collect more under the lands compared to the cloth DM. Secondly, the paper DM is originally 70 μm thinner, leaving less volume for stored liquid water. This is likely why the cloth performed better at higher current densities.

Current effect.— Figure 9 shows the water content vs current density for four tests (Tests 1, 3, 5, and 9) that are all at constant flow, constant humidity, and increasing current conditions for each DM material. The curves both have a minimum water content at 0.35 A/cm^2 and a maximum at 1.0 A/cm^2. It is believed to be a result of the complex interaction between channel level drag and slug removal, heat transfer, evaporation/condensation, and electrochemical processes. No monotonic relationship is observed because

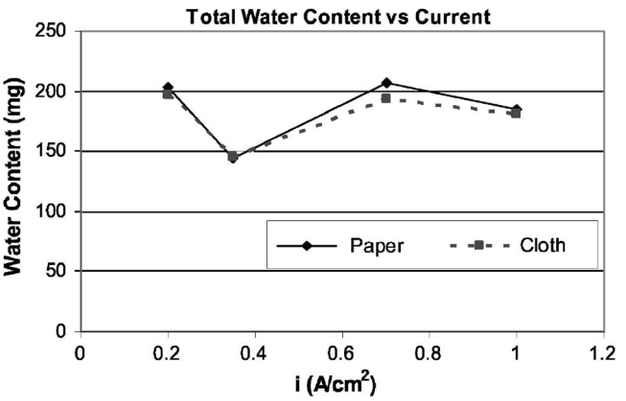

Figure 9. Relationship of water content with current density. Test conditions: T_{cell} = 80°C, P_{cell} = 0.1 MPag, Flow rate A/C = 174/417 sccm, RH A/C = 90/80°C.

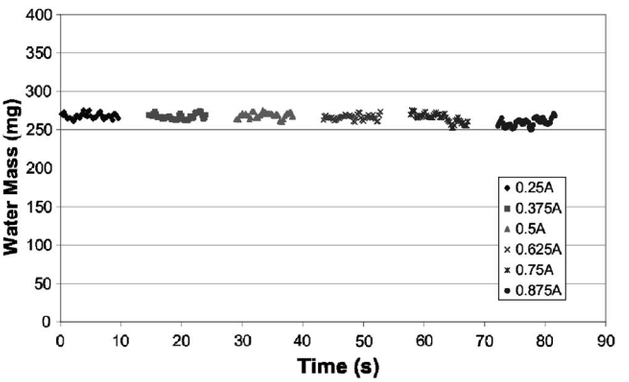

Figure 11. Transient test from 0.2 to 0.7 cm^2 incrementing by 0.1 A/cm^2 every 10 s, for cloth DM. (5 s pause before each step to change current). Test conditions: T_{cell} = 80°C, P_{cell} = 0.1 MPag, Flow rate A/C = 174/417 sccm, RH A/C = 90/80°C.

more than one physicochemical process is present. However, there is no conclusive trend between water mass and current density, although both DM materials show trends consistent with each other. This is noteworthy because the two materials showed such different characteristics concerning water distribution and flooding losses.

Transient tests.— From Faraday's law, the rate of water generation has a linear relationship with the operating current or current density. Because the current was increased during these tests while the flow rates remained constant, the liquid-water mass in the cell should increase in a linear fashion with current density under load transients, as long as the fraction of water generated that condenses to liquid and is stored in the fuel cell remains constant. In steady state, a nonmonotonic relationship was shown between current and stored liquid mass, but in those tests the flow rate was constant at a given current density, so that channel velocity increased with increasing current density. In the set of transient tests listed in Table II, the flow rate was constant during load cycling, and not enough time was given between cycles to allow a true steady state to emerge. Figures 10-12 show the liquid-water mass vs time plots for the 1, 10, and 20 s per step, respectively, for the cloth transient tests at fully humidified low flow (A/C = 174/417 sccm) conditions. The 1 and 10 s per step tests show a roughly constant water mass vs time relationship. The 20 s per step test was the only way to show any increase in liquid water content. Toward the end of the test, the slopes of the liquid-water mass vs time at each increment increase. For the cell to generate 10 mg of water, the time required at 0.2 and 0.7 A/cm^2 is 43 and 12 s, respectively (calculation shown in Appendix B). Thus, a 1 s step change should not show any increase in water mass. The 10 s per step test may show some increase at high current density only and a 20 s per step test should show some increase in the water mass. In summary, both experiment and calculation reveal the time scale for significant liquid water storage changes in the fuel cell under load cycling is tens of seconds to minutes, which is also consistent with dynamic performance observation under flooding conditions.[33]

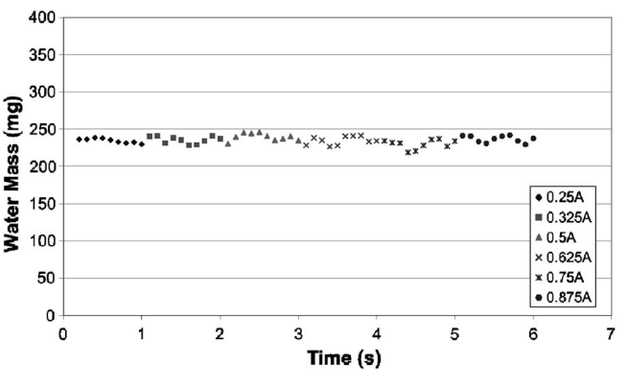

Figure 10. Transient test from 0.2 to 0.7 A/cm^2 incrementing by 0.1 A/cm^2 every 1 s, for cloth DM. Test conditions: T_{cell} = 80°C, P_{cell} = 0.1 MPag, Flow rate A/C = 174/417 sccm, RH A/C = 90/80°C.

Conclusions

Various steady-state and transient tests were performed to evaluate the water storage distribution and removal in a 12.5 cm^2 fuel cell using either a hydrophobic carbon fiber paper or cloth DM. Neutron imaging was used to measure the liquid water content in the cell to examine the relationship water content has with performance, DM material, humidity conditions, current, and flow rate. The water content showed no monotonic trend with current density but decreased with increasing flow rate in the channels and under the lands. The steady-state water decrease under the lands for a given increase in flow rate was greater for the cloth DM than the paper DM for all current densities. The two different diffusion media materials also exhibited clearly different performance and water distributions over a wide range of operating conditions. In the paper DM, flooding losses occurred at lower current density, and water tended to be in the DM under the lands more than in the channel locations, with

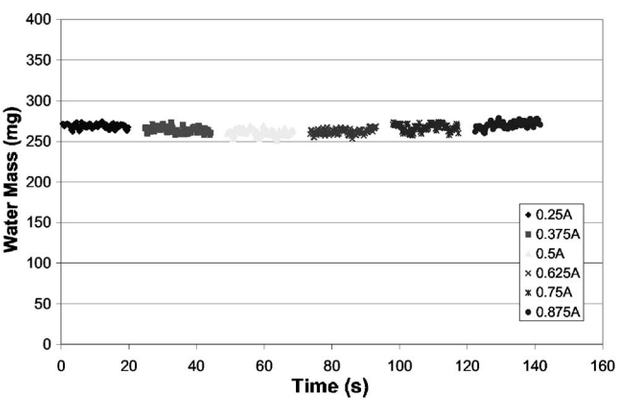

Figure 12. Transient test from 0.2 to 0.7 A/cm^2 incrementing by 0.1 A/cm^2 every 20 s, for cloth DM. (5 s pause before each step to change current). Test conditions: T_{cell} = 80°C, P_{cell} = 0.1 MPag, Flow rate A/C = 174/417 sccm, RH A/C = 90/80°C.

about 60% of the water in the landings and 40% in or under the channel. The cloth DM, however, has a more balanced 50:50 landing to channel water distribution. When these results were normalized on a volume basis, the paper DM averaged 174% of the water content under the lands, compared to the cloth DM, resulting in a much greater liquid saturation in the cloth DM. Polarization curve results confirmed this increased water storage caused a flooding performance loss for the paper DM. Experiment and calculation reveal the time scale for significant liquid-water storage changes in the fuel cell under load cycling is tens of seconds to minutes.

Acknowledgments

The authors thank the industrial source of funding for sponsorship of this work.

The Pennsylvania State University assisted in meeting the publication costs of this article.

Appendix A
Calculation of Effective Porosity

Test 1, cloth DM.—

$$\varepsilon_{comp} = 0.625$$

$$A_{total} = 12.5\ cm^2$$

Because the channel-to-landing ratio is 1, the fraction of area occupied by landings is

$$f = 6/13 = 0.462$$

$$A_{lands} = f \times A_{total} = (0.462) \times (12.5\ cm^2) = 5.78\ cm^2$$

$$t_{DM} = 250\ \mu m = 0.025\ cm$$

$$m_{H_2O,lands} = 100\ mg$$

$$\rho_{H_2O} = 1000\ mg/cm^3$$

$$\varepsilon_{eff} = \left[1 - \frac{m_{H_2O,lands}}{\varepsilon_{comp}\rho_{H_2O}A_{lands}t_{DM}}\right]\varepsilon_{comp} = \left[1 - \frac{(100\ mg)}{(0.625)\left(1000\frac{mg}{cm^3}\right)(5.78\ cm^2)(0.025\ cm)}\right](0.625) \approx -0.067$$

All the liquid water under the lands was assumed to be on one side of the fuel cell, so a negative value means that some water must be in the other side of the DM.

Appendix B
Calculation of Effective Porosity

Water generation time scale calculation.— Assuming it takes 10 mg of liquid water to detect a change in water mass by the neutron radiography system, the time the fuel cell takes to generate that water for a given current density can be found by using Faraday's law

$$m_{H_2O} = 10\ mg\ (assumed)$$

$$MW_{H_2O} = 18\ g/mol$$

$$n = 2\frac{e^-\ eg}{mol}$$

$$F = 96485\frac{C}{e^-\ eq}$$

$$A_{total} = 12.5\ cm^2$$

$$\Delta t = \frac{N_{H_2O}}{\dot{N}_{H_2O}} = \frac{m_{H_2O}}{MW_{H_2O}}\frac{nF}{iA_{total}}$$

$$\Delta t\left(i = 0.2\frac{A}{cm^2}\right) = \frac{(10\ mg)}{\left(18\frac{g}{mol}\right)}\frac{\left(2\frac{e^-\ eq}{mol}\right)\left(96485\frac{C}{e^-\ eq}\right)}{\left(0.2\frac{A}{cm^2}\right)(12.532\ cm^2)}\left(\frac{1\ g}{1000\ mg}\right) \approx 43\ s$$

$$\Delta t\left(i = 0.7\frac{A}{cm^2}\right) = \frac{(10\ mg)}{\left(18\frac{g}{mol}\right)}\frac{\left(2\frac{e^-\ eq}{mol}\right)\left(96485\frac{C}{e^-\ eq}\right)}{\left(0.2\frac{A}{cm^2}\right)(12.532\ cm^2)}\left(\frac{1\ g}{1000\ mg}\right) \approx 12\ s$$

List of Symbols

A_{lands}	area under the landings, cm^2
A_{total}	total fuel cell active area, cm^2
F	Faraday's constant, 96485, C/e^-eq
f	fraction of total area occupied by landings
MW_{H_2O}	molecular weight of water, g/mol
$m_{H_2O,high}$	mass of water in the cell at the high flow rate, mg
$m_{H_2O,low}$	mass of water in the cell at the low flow rate, mg
$m_{H_2O,lands}$	mass of water under the landings, mg
n	equivalent electrons per mol of species produced or consumed, e^-eq/mol
t_{DM}	thickness of the diffusion media, cm
ρ_{H_2O}	density of water, mg/cm^3
ε_{eff}	effective porosity
ε_{comp}	compressed porosity

References

1. A. Turhan, K. Heller, J. Brenizer, and M. M. Mench, Submitted to *J. Power Sources*, In press.
2. H. Yamada, T. Hatanaka, and Y. Morimoto, Abstract 1516, The Electrochemical Society Meeting Abstracts, Vol. 2005-1, Quebec City, Canada, May 15–20, 2005.
3. J. Larminie and A. Dicks, *Fuel Cell Systems Explained*, 2nd ed., p. 67–94, John Wiley & Sons, Ltd., West Sussex, England (2003).
4. M. F. Mathias, J. Roth, J. Fleming, and W. Lehnert, *Handbook of Fuel Cells—Fundamentals, Technology and Applications*, Chap. 42, Vol. 3, W. Vielstich, A. Lamm, and H. A. Gasteiger, Editors, John Wiley & Sons, Ltd., New York (2003).
5. L. You and H. Liu, *Int. J. Heat Mass Transfer*, **45**, 2277 (2002).
6. Z. H. Wang, C. Y. Wang, and K. S. Chen, *J. Power Sources*, **94**, 40 (2001).
7. D. Natarajan and T. V. Nguyen, *J. Electrochem. Soc.*, **148**, A1324 (2001).
8. L. You and H. Liu, *Int. J. Heat Mass Transfer*, **45**, 2277 (2002).
9. U. Pasaogullari and C. Y. Wang, *J. Electrochem. Soc.*, **152**, A380 (2005).
10. U. Pasaogullari, C. Y. Wang, and K. S. Chen, *J. Electrochem. Soc.*, **152**, A1574 (2005).
11. C. Ziegler, H. M. Yu, and J. O. Schumacher, *J. Electrochem. Soc.*, **152**, A1555 (2005).
12. S. Mazumder and J. V. Cole, *J. Electrochem. Soc.*, **150**, A1503 (2003).
13. P. Berg, K. Promislow, J. St. Pierre, J. Stumper, and B. Wetton, *J. Electrochem. Soc.*, **151**, A341 (2004).
14. E. Birgersson, M. Noponen, and M. Vynnycky, *J. Electrochem. Soc.*, **152**, A1021 (2005).
15. D. Natarajan and T. V. Nguyen, *J. Electrochem. Soc.*, **148**, A1324 (2001).
16. A. A. Kulikovsky, *J. Electrochem. Soc.*, **150**, A1432 (2003).
17. A. Z. Weber, R. M. Darling, and J. Newman, *J. Electrochem. Soc.*, **151**, A1715 (2004).
18. T. Berning and N. Djilali, *J. Electrochem. Soc.*, **150**, A1589 (2003).
19. G. Lin, W. He, and T. V. Nguyen, *J. Electrochem. Soc.*, **151**, A1999 (2004).
20. H. Meng and C. Y. Wang, *J. Electrochem. Soc.*, **152**, A1733 (2005).
21. J. Yi and T. V. Nguyen, *J. Electrochem. Soc.*, **146**, 38 (1999).
22. K. W. Feindel, L. P.-A. LaRocque, D. Starke, S. H. Bergens, and R. E. Wasylishen, *J. Am. Chem. Soc.*, **126**, 11436 (2004).
23. S. Litster, D. Sinton, and N. Djilali, *J. Power Sources*, **154**, 95 (2006).
24. S. Tsushima, K. Teranishi, and S. Harai, *Electrochem. Solid-State Lett.*, **7**, A269 (2004).
25. K. Tüber, D. Pócza, and C. Hebling, *J. Power Sources*, **124**, 403 (2003).
26. R. J. Bellows, M. Y. Lin, M. Arif, A. K. Thompson, and D. Jacobson, *J. Electrochem. Soc.*, **146**, 1099 (1999).
27. A. B. Geiger, A. Tsukada, E. Lehmann, P. Vontobel, A. Wokaun, and G. G. Scherer, *Fuel Cells*, **2**, 92 (2002).
28. D. Kramer, J. Zhang, R. Shimoi, E. Lehmann, A. Wokaun, K. Shinohara, and G. Scherer, *Electrochim. Acta*, **50**, 2603 (2005).
29. N. Pekula, K. Heller, P. A. Chuang, A. Turhan, M. M. Mench, J. S. Brenizer, and K. Ünlü, *Nucl. Instrum. Methods Phys. Res. A*, **542**, 134 (2005).
30. R. Satija, D. L. Jacobson, M. Arif, and S. A. Werner, *J. Power Sources*, **129**, 238 (2004).
31. K. Heller, P. A. Chuang, J. Brenizer, and K. Ünlü, *Amer. Nuc. Soc. Trans.*, **93**, 860 (2005).
32. J. S. Brenizer, K. W. Tobin, J. M. Hylko, D. D. McRae, and R. W. Jenkins, Jr., *Mater. Eval.*, **45**, 1310 (1987).
33. M. M. Mench and C. Y. Wang, *J. Electrochem. Soc.*, **150**, A79 (2003).